

ALMA Memo #281

Development of a Pulse Tube Refrigerator for Millimeter Array Sensor Cooling: Phase I*

Ray Radebaugh⁽¹⁾

Eric Marquardt⁽¹⁾

Peter Bradley⁽¹⁾

⁽¹⁾National Institute of Standards and Technology

* Contribution of NIST, not subject to copyright in the U.S.

DEVELOPMENT OF A PULSE TUBE REFRIGERATOR FOR MILLIMETER ARRAY SENSOR COOLING: PHASE I*

Progress Report for April to September, 1999

Prepared by: Ray Radebaugh, Eric Marquardt, and Peter Bradley
Cryogenic Technologies Group
Physical and Chemical Properties Division
National Institute of Standards and Technology
325 Broadway
Boulder, CO 80303 E-mail: radebaugh@boulder.nist.gov

Submitted to: Larry D'Addario
National Radio Astronomy Observatory (NRAO)
949 North Cherry Ave.
Tucson, AZ 85721-0655

October 20, 1999

Abstract. This report describes progress made between April, 1999, and September, 1999, in a research and development program regarding pulse tube refrigeration at 10 K for high efficiency and high reliability sensor cooling applications. The particular application being addressed here is one in which a pulse tube refrigerator is used to precool a helium Joule-Thomson stage to 10 K. The Joule-Thomson stage is designed to reach 3.8 K for cooling Superconductor-Insulator-Superconductor (SIS) radio frequency detectors on the Atacama Large Millimeter Array (ALMA) radio telescope to be located in the Andes Mountains of northern Chile. The remote location requires high efficiency and high reliability for the refrigeration system.

The program described here is sponsored by the National Radio Astronomy Observatory (NRAO) and is intended to determine the feasibility of operating pulse tube refrigerators with valveless compressors (pressure oscillators) incorporating flexure bearings for long life. The use of a valveless compressor to drive a pulse tube refrigerator leads to an inherently high efficiency system, but frequencies must be at least 30 Hz to reduce the compressor to acceptable size. The operation of regenerators at 30 Hz or higher at temperatures as low as 10 K has not previously been investigated. A better understanding and optimization of the heat transfer processes inside the regenerator are required in order to maintain high system efficiency. The modeling and optimization carried out in this phase of the program shows that the required 2 W of refrigeration at 10 K would require about 1400 W of input power to the two-stage pulse tube refrigerator, well within the maximum allowed value of 2000 W. The input power is shown to be a strong function of the figure-of-merit of the second stage pulse tube, for which a value of 0.8 was assumed based on experiments made at higher temperatures. A test apparatus designed to measure the performance of the second stage regenerator and pulse tube is described. Such measurements are to be carried out in Phase II.

* Contribution of NIST, not subject to copyright in the U. S.

Introduction. This report describes progress made between April, 1999, and September, 1999, in a research and development program regarding pulse tube refrigeration at 10 K for high efficiency and high reliability sensor cooling applications. The goal of this research is to develop the precooling technology required as part of the sensor cooling for the Atacama Large Millimeter Array (ALMA). This radio telescope is designed for wavelengths from approximately 0.4 mm to 10 mm. It will consist of at least 64 antennas, each 12 m in diameter and distributed over a 3 to 10 km diameter circle on the remote, high altitude Atacama Desert in the Andes Mountains of northern Chile. This effort is part of the Design and Development Phase for ALMA, funded by the National Science Foundation and managed by the National Radio Astronomy Observatory (NRAO). The main objectives are to achieve substantial improvements in power efficiency, reliability, and maintenance effort compared with off-the-self refrigeration systems at the same load temperatures and capacities. A secondary objective is to tailor the capacities more closely to the ALMA requirements than is possible with available products.

The sensors for ALMA are made with Superconductor-Insulator-Superconductor (SIS) junctions that must be cooled to about 3.8 K to achieve the greatest sensitivity for millimeter radiation. A helium Joule-Thomson refrigerator will be used for the final stage of cooling to 3.8 K. Sub-atmospheric pressure is required on the return low-pressure line to achieve 3.8 K. The refrigeration power available with a Joule-Thomson cryocooler is given by

$$\dot{Q}_c = \dot{m}\Delta h_{\min}, \quad (1)$$

where \dot{m} is mass flow rate and Δh_{\min} is the minimum value of the difference in the specific enthalpy between the low and high pressures over the temperature range spanned by the heat exchanger. Figure 1 shows the specific enthalpy of helium versus temperature for several

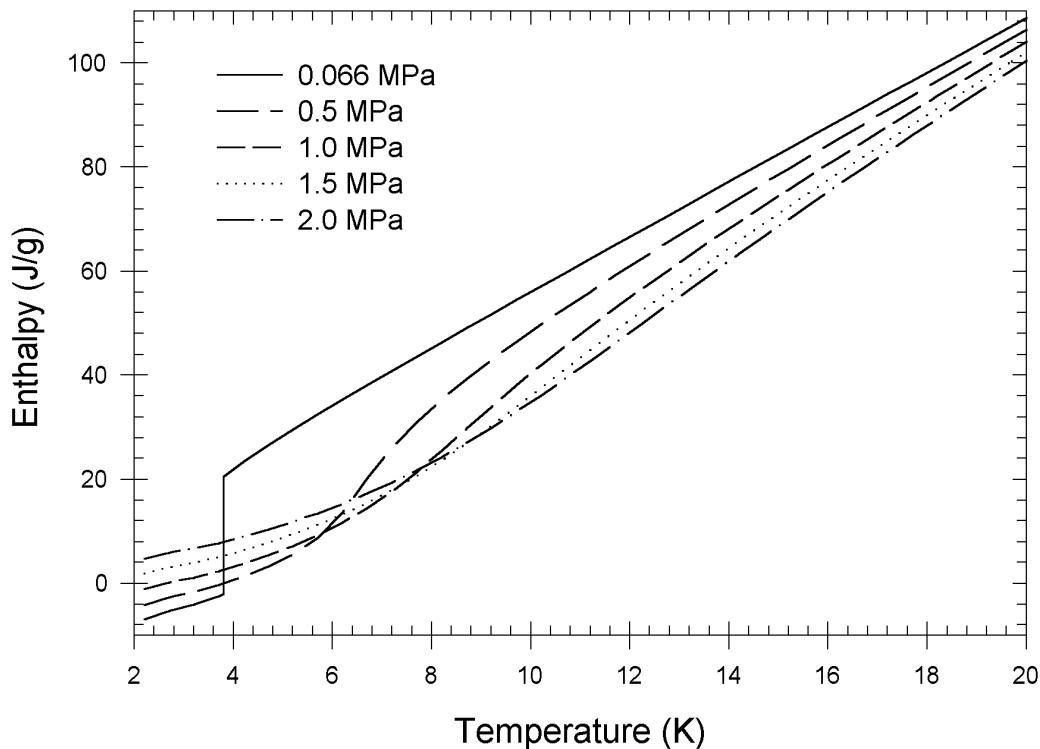


Figure 1. Specific enthalpy of helium.

different pressures, including the vapor pressure of helium at 3.8 K (0.066 MPa). The minimum enthalpy difference between, for example, 0.066 MPa and 1.5 MPa approximately doubles as the high temperature end (precooling temperature) is lowered from 20 K to 12.5 K. Thus, a precooling temperature of 12.5 K leads to high efficiency in the Joule-Thomson stage. Precooling to 12.5 K must be performed with a separate refrigerator operating at about 10 K to account for some temperature difference to transfer heat between the two systems. This report describes progress on research aimed at developing the precooling refrigerator.

The precooling refrigerator must provide cooling at two temperatures, as given by

Stage 1: 16 W at 60 to 80 K
 Stage 2: 3.5 W at 15 K, or
 2.0 W at 10 K (preferred).

Other specifications for this refrigerator are given in Table 1. Cooling at 80 K for Stage 1 is for a radiation shield and current leads. Temperatures lower than 80 K for this first stage would be

Table 1: Specifications		
General description: Two-temperature cryocooler		
	Stage 1	Stage 2
No-load temperatures, max	70 K	12 K
Full-load* temperatures, max	90 K	15 K
*(both stages simultaneously)		
Loads (full)	16 W 3.5 W at 15 K or 2.0 W at 10 K (preferred)	
Configuration: Either integral or split compressor, but use of integral compressor results in additional constraints as given below.		
Heat rejection: To 293 K ambient air, with rejection point at least 6 m from the refrigeration points. If compressor is integral with refrigerator, a secondary circuit (e.g., H ₂ O) should be provided to transfer heat to the remote rejection point.		
Orientation: Specifications must be met over a 90 deg range of orientation of refrigerator with respect to gravity. If the compressor is separate, it may have a fixed orientation with respect to gravity.		
Power consumption at full load, max:	2000 W	
Power consumption at full load, design goals:	1100 W	
Sizes, max: Refrigerator (including components in a vacuum chamber)	20 cm dia x 50 cm long	
components outside vacuum chamber:		
"above" (see text)	volume	0.025 m ³
	largest dimen.	0.4 m
"below"	volume	0.05 m ³
	largest dimen.	0.7 m
split compressor	no restrictions	
Reliability: The design should be expected to meet the performance specifications during at least 2 years of continuous operation, without the need for maintenance operations on any components. Maintenance-free operation for 3 to 5 years is a desirable goal.		

necessary only if it improved the overall efficiency of the refrigerator, such as by improving the second-stage performance. A two-stage pulse tube refrigerator has been selected for this study because it offers the advantage of high efficiency, high reliability, and low cost. A disadvantage is the sensitivity to orientation in gravity. Ideally the cold end of the pulse tube should be down to prevent a gravitational convective instability. Previous research has shown that the instability depends on the pulse tube diameter. It should also be a function of the operating frequency as well as several other parameters. Thus, the research described here provides for testing at various orientations. Current models of pulse tube refrigerators are not able to predict the orientation dependence. Cryocoolers and pulse tube refrigeration have been reviewed by Radebaugh [1, 2, 3].

Existing Commercial Cryocoolers. Figure 2 gives the schematics of the three common recuperative cryocooler cycles and Fig. 3 gives the schematics of the three common regenerative cryocooler cycles. In Fig. 3 the pulse tube is shown as driven with a valveless compressor. It also can be driven with a valved (Gifford-McMahon) compressor. Figure 4 gives a map in terms of refrigeration power and temperature for various refrigerator types. The ALMA cooling requirements are close to those of cryopumps, except that a somewhat lower temperature is required for the ALMA application. The cryopump application is a large one that requires the manufacture of two-stage Gifford-McMahon refrigerators at a rate of about 20,000/year. The cost of these refrigerators is in the range of \$10,000 to \$20,000 each. These refrigerators are rather inefficient and would require about 3 kW of input power to meet the cooling requirements for the ALMA application. In addition, they require nearly yearly maintenance. A two-stage pulse tube refrigerator has just been introduced commercially since last July, but currently it requires more input power than the Gifford McMahon refrigerator for the same refrigeration power. Currently all commercial two stage cryocoolers utilize valved (Gifford-McMahon) compressors to maintain low cost. The irreversible expansion in the valves results in low

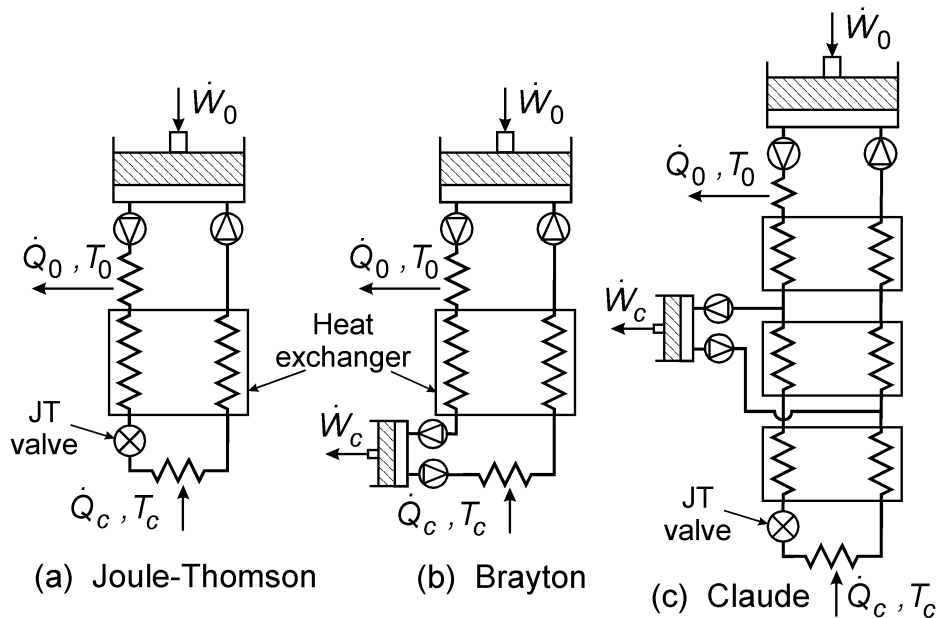


Figure 2. Schematics of three common recuperative (steady flow) cycles.

efficiency. The coldhead of these commercial two-stage cryocoolers generally operates at very low frequencies of about 1 Hz. These Gifford-McMahon refrigerators are capable of reaching very low temperatures, even below 4 K, but the efficiency is low.

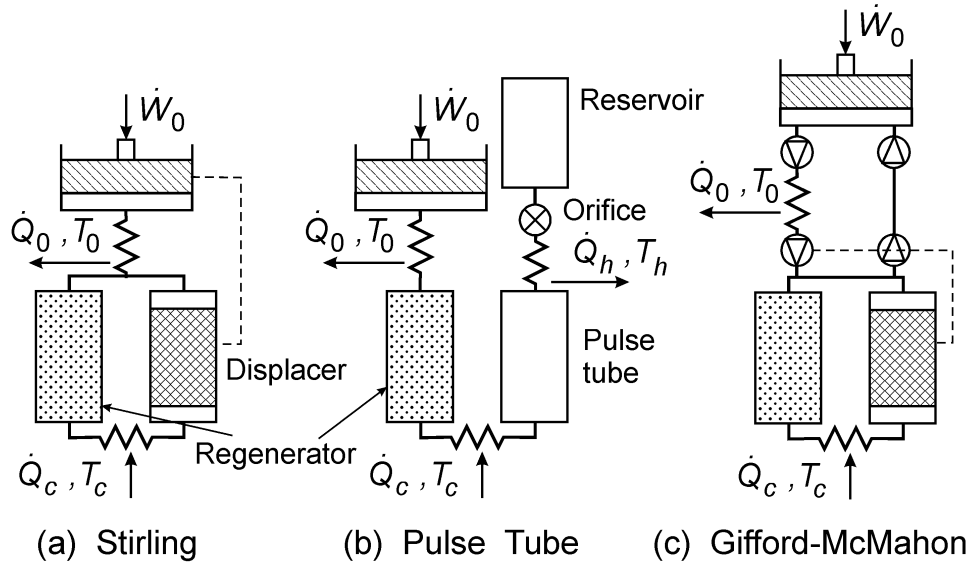


Figure 3. Schematics of three common regenerative (oscillating flow) cycles.

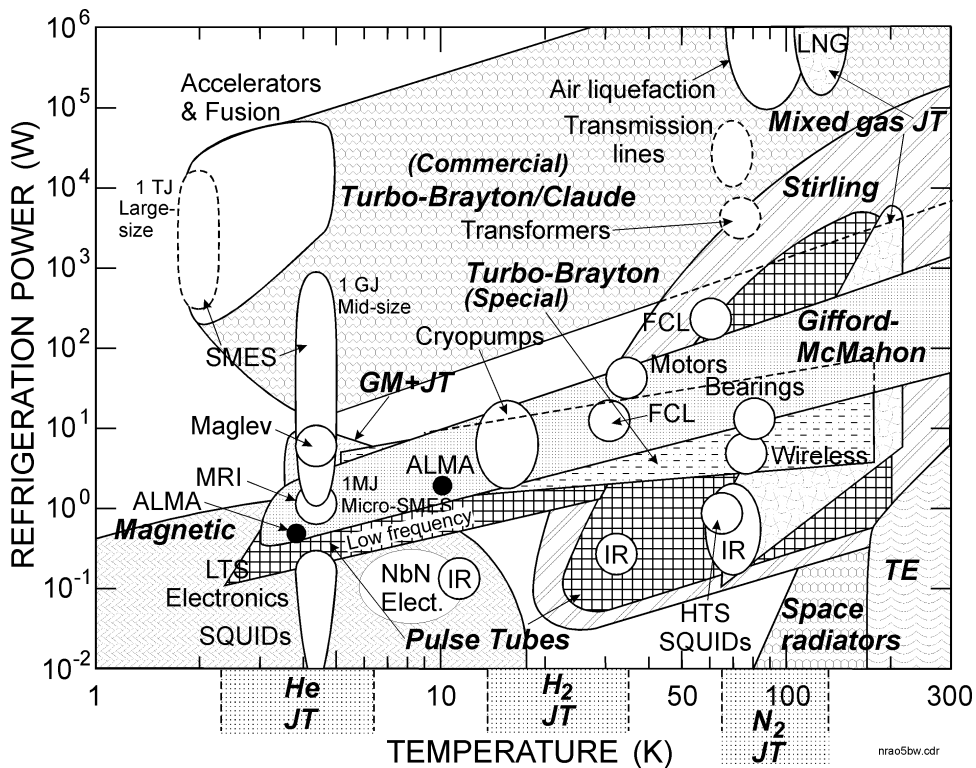


Figure 4. Map of cryocooler applications and cryocooler types

Valveless compressors must be oil-free because the dead volume associated with any oil removal equipment would undergo a pressure oscillation and necessitate a much greater swept volume in the compressor. Lifetimes of oil-free compressors are usually limited to about 5000 hours of continuous use unless flexure bearings are used to support the piston in the cylinder with no contact. Figure 5 shows a schematic of a linear compressor with two types of flexure bearings. These compressors have been used to drive Stirling and pulse tube refrigerators for space applications in the last few years. They have demonstrated 10 years of continuous operation with no maintenance. When operated at resonance conditions, a well designed linear compressor can achieve an efficiency of 85% in the conversion of electrical power to PV power. In contrast, a valved compressor typically achieves an efficiency of 50%. Figure 6 compares the efficiency of various one-stage cryocoolers operating at about 80 K. This figure shows that the pulse tube refrigerator driven with a valveless compressor has become the most efficient cryocooler for temperatures around 80 K. Efficiencies near 20% of Carnot at 80 K are now possible with pulse tube refrigerators when driven with valveless compressors of 85% efficiency.

The use of valveless (Stirling-type) compressors or pressure oscillators improves the efficiency, but they must be oil-free. With no valves to separate the cold head and the compressor, the cold head must operate at the same frequency as the compressor. To maintain a reasonably compact compressor, the operating frequency should be about 20 Hz or above. The performance of regenerators at this high frequency and at temperatures below about 20 K has not been studied in much detail. This low temperature, high frequency regenerator operation has recently become of much interest to many researchers in the field. There are some indications that the regenerator is not able to transfer the heat quickly enough at this low temperature. If this problem can be overcome, the 10 K refrigeration requirement of ALMA could be accomplished with high efficiency and high reliability by using a pulse tube refrigerator driven with a valveless compressor. Flexure bearing compressors were initially very expensive when developed for satellite applications, but recently some commercial versions have been developed at much lower costs.

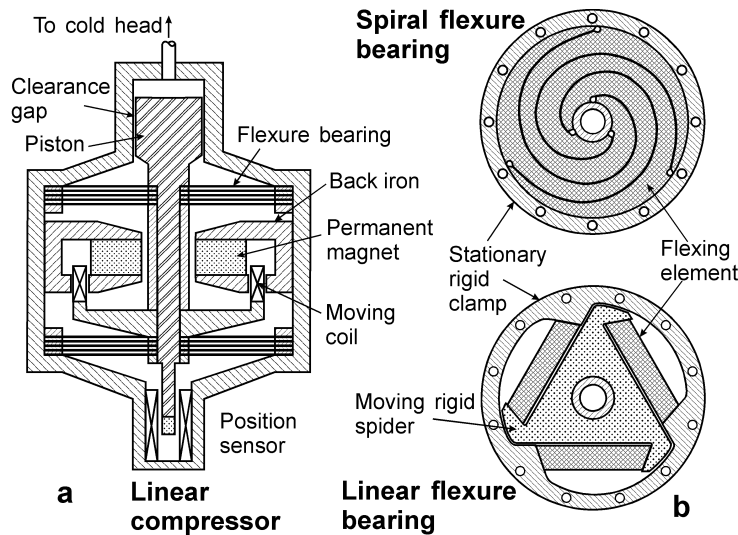


Figure 5. (a) Cross-section of a linear compressor with (b) two types of flexure bearings.

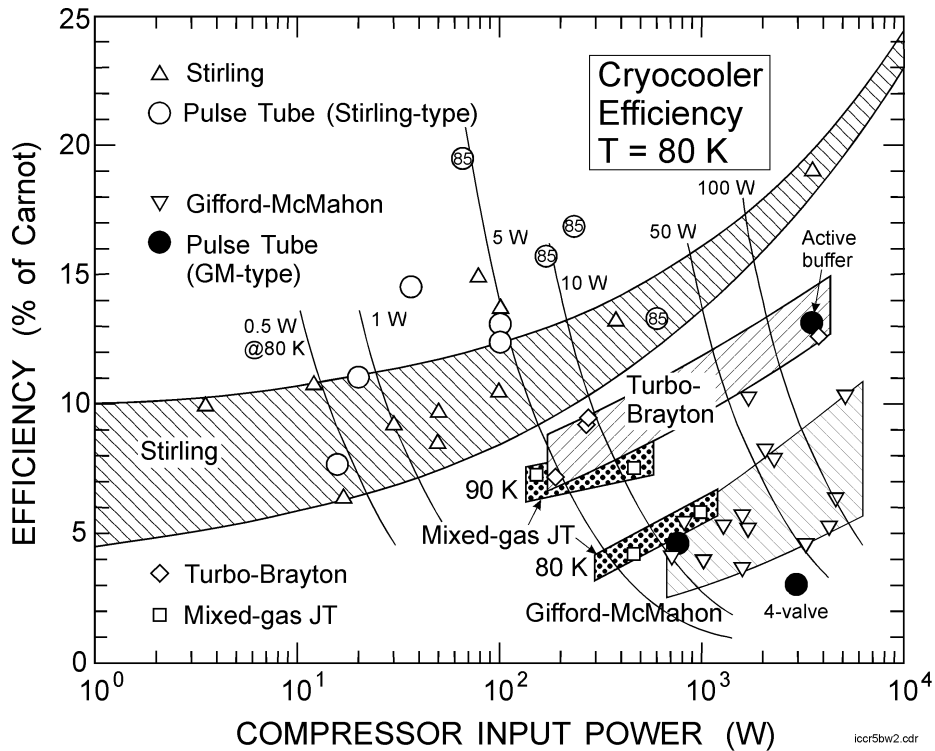


Figure 4. Carnot efficiency of various cryocooler types at 80 K.

Two-Stage Pulse Tube Refrigerators. Figure 7 shows the conventional arrangement of the two pulse tube stages when temperatures below about 30 K are needed. Normally the warm end of the second stage pulse tube is allowed to reject heat to ambient. However, if the large temperature difference in the second stage pulse tube leads to a large enough loss in this pulse

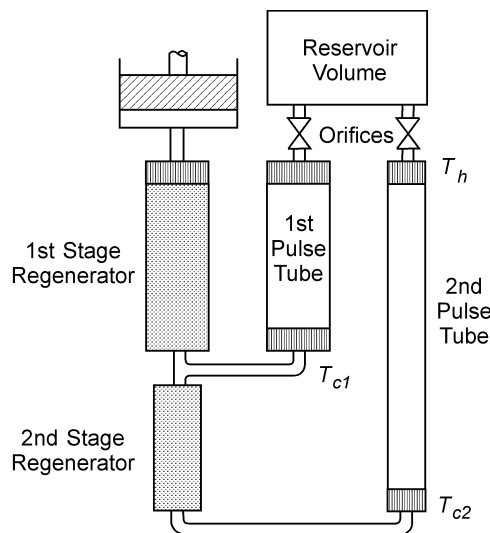


Figure 7. Schematic of a two-stage pulse tube refrigerator with second-stage pulse tube heat sink to ambient.

tube, it may be more advantageous to heat sink it to the first stage. The staging arrangement also depends on the efficiency of the two stages. Some calculations are done here to investigate the two possible options regarding the heat sinking of the second-stage pulse tube.

Statement of Work. There are two major questions that need to be answered in regard to using a pulse tube refrigerator for this application. The first is the operation of the second stage regenerator at temperatures down to 10 to 15 K with frequencies of about 30 Hz or more. Little is known about the efficient operation of regenerators at these low temperatures with such high frequencies. The high frequency operation is required to achieve high efficiency with a compact compressor. The second major question regarding the use of pulse tube refrigerators is the ability to operate over the 0 to 90 degree orientation as opposed to a -45 to $+45$ degree orientation. The research plan has been structured to answer these questions as quickly as possible before proceeding with other phases of the program.

1. Perform detailed modeling and optimization of complete two-stage pulse tube refrigerator. Various models will be used in this effort and will include the use of REGEN3.1. This modeling effort will provide the calculated optimum geometry for the two regenerators, the two pulse tubes (including tapers), the necessary heat exchangers, the orifice settings, the inertance tubes, reservoir volumes, and compressor swept volume.
2. Perform the detailed design of the vacuum test chamber and support system required to conduct experiments at angles between 0 and 90 degrees.
3. Order vacuum test chamber (NIST funds to be used for vacuum chamber).
4. Order two flexure bearing compressor modules designed for operation at 30 Hz and providing at least 1400 W of PV power. Two modules would be mounted in a back-to-back arrangement to eliminate vibration and would provide the power required of the two-stage pulse tube refrigerator. (NIST funds to be used for compressor)
5. Perform detailed design with parts drawings for all test bed components.
6. Perform detailed design with parts drawings for pulse tube refrigerator components.
7. Fabricate pulse tube refrigerator components for testing second stage (includes optimized second stage regenerator, regenerator for precooling, second stage pulse tube, heat exchangers, inertance tube, orifices, and reservoir volume). (Does not include some test bed components required for testing second-stage pulse tube.)

Modeling. The performance of regenerators at 10 K is generally hampered by the low volumetric heat capacity of matrix materials at this low temperature. For the past several years, 4 K Gifford-McMahon and pulse tube refrigerators have been investigated and built by several research organizations and companies. Such systems are now commercially available. However, all of these 4 K systems operate at about 2 Hz or less, which requires the use of a rotary valve and a valved compressor and results in low efficiency. Valveless compressors have an inherently much higher efficiency, but must operate at frequencies of about 30 Hz or higher to be sufficiently compact for practical use. The performance of regenerators generally deteriorates as the frequency is increased, but for temperatures of about 50 K or higher, operation at 30 to 60 Hz has been quite successful and led to pulse tube refrigerators of very high efficiency (as high as 15 to 20% of Carnot at 80 K). Little is known about the behavior of regenerators at lower temperatures at these high frequencies.

The first item considered in operating regenerators at lower temperatures is the effect of thermal penetration depths in both the solid matrix and in the helium gas. To provide adequate thermal contact with the gas, the gas channel must have hydraulic diameters comparable to or less than the thermal penetration depth in the gas for the particular frequency of interest. The characteristic matrix dimension (particle diameter, wire diameter, plate thickness) should not be larger than the thermal penetration depth in the solid to avoid having matrix not contributing to the effective heat capacity but adding to the axial thermal conduction. The thermal penetration depth in a semi-infinite medium is given by

$$d_t = \sqrt{k/rcpf}, \quad (2)$$

where k is the thermal conductivity, r is the density, c is the specific heat, and f is the frequency. For a frequency of 30 Hz the thermal penetration depth in helium at a pressure of 3 MPa varies from about 300 μm at 300 K to about 30 μm at 10 K. The pressure dependence is small but higher pressures tend to decrease the thermal penetration depth. For use up to 300 K 325-mesh screen is typically used in regenerators operating at 30 Hz and is found to be about the optimum mesh size for this frequency. Such screen has a hydraulic diameter of 64 μm , which is significantly less than the 300 μm thermal penetration depth in helium at 300 K. The thermal penetration depth in stainless steel at temperatures from 80 to 300 K is about 200 μm . The wire diameter of 325 mesh is 36 μm . Thus, all of the wire is contributing toward the effective heat capacity.

At 10 K the thermal penetration depth in most of the rare earth materials used for high heat capacity is about 250 μm . In order to obtain the highest possible matrix heat capacity at 10 K, a matrix characteristic dimension of about 250 μm should be used. The gas channel should have a hydraulic diameter comparable to the thermal penetration depth, which is about 30 μm at 10 K. Thus, for a parallel plate geometry the optimum porosity would be about 10% at 10 K. This porosity is much less than the 68% porosity that occurs in most screen regenerators. The simple argument given above for matrix dimensions should be regarded only as a first approximation toward any optimization since it does not take into account any viscous losses or axial thermal conduction. Those losses are considered only in more sophisticated models, such as REGEN3.1 developed by NIST for modeling the performance of regenerators. REGEN3.1 uses a finite difference calculation and incorporates the NIST equations for the real gas properties of helium. Very few assumptions are made in this model, and it is usually considered the most accurate model for regenerator performance, although running times are long. This model was used to optimize the parameters of a regenerator operating between 10 and 80 K for a frequency of 30 Hz to investigate the feasibility of operating a regenerator at these low temperatures and high frequencies. A total of 54 runs of REGEN3.1 have been made to date. The parameters chosen for the first run are a result of some previous studies that allowed us to obtain values near the optimum. These initial parameters are as follows:

Pulse tube figure of merit: 0.80
 Cold temperature: 10 K
 Warm temperature: 80 K
 Average pressure: 3.0 MPa
 Pressure ratio: 1.3

Gas: helium, real gas properties
Configuration: packed spheres
Porosity: 0.38
Hydraulic diameter: 32.7 μm (80 μm spheres)
Total cross-sectional area: 4.10 cm^2
Length: 35 mm
Material: Pb+5%Sb
Conductivity reduction factor: 0.05
Frequency: 30 Hz
Cold end mass flow: 5.30 g/s
Phase between cold end mass flow and pressure: -15°

The flow rate chosen was rather arbitrary, but once an optimum geometry is found the parameters are independent of flow rate as long as the ratio of cross-sectional area to the flow rate remains the same. After each run one or more of these parameters were changed to observe the effect on the refrigeration power, the COP, and various other parameters.

A summary of the 54 REGEN3.1 runs leading to an optimization of the regenerator is given in Table 2. In this table the phase angle ϕ is the phase by which the mass flow at the warm end leads the pressure. When this phase angle begins to increase beyond about 25° , the required compressor swept volume begins to increase significantly. This phase angle is directly proportional to the gas volume in the regenerator. A larger regenerator contributes more heat capacity, but at the expense of requiring a larger compressor. The COP given here refers to the ratio of the net refrigeration power divided by the isothermal PV power at 80 K required to drive the flow into the warm end of the second stage regenerator. A first stage would be needed to go to 300 K. The first stage was optimized with another set of REGEN3.1 runs using stainless steel screen as the regenerator matrix.

Table 3 lists the general trends and conclusions that can be reached from the REGEN3.1 runs made to date for the second stage. Note that the use of a high heat capacity material Er_3Co is required to obtain a reasonable COP at 10 K. Packed spheres can provide a reasonable COP at 30 Hz, but only if the sphere size is about 80 μm . Parallel plates of lower porosity have not been studied yet and offer the potential of much higher COPs. Screens gave poorer performance than packed spheres. The effect of lower warm end temperatures has not been studied, except for a few runs where the warm end was 30 K. Though much higher refrigeration powers were obtained when the warm end was at 30 K compared with 80 K, the overall system performance was about the same as that for 80 K. The REGEN3.1 calculations showed that Er_3Co spheres gave much better performance than did Pb+5%Sb spheres. However, further increases in the matrix heat capacity had little effect in improving the performance. The volumetric heat capacity of Er_3Co exceeds that of Pb+5%Sb at temperatures below about 17 K.

Table 2. Summary of REGEN3.1 runs

Tc = 10 K, Th = 80 K (*unless italics or different font*)

Try #	Run #	Input comments	\dot{Q}_{net} ,	COP,	ϕ ,	Other results
1	2583	Similar to #2529 except Tc=10 K	0.22	0.0055	37.8	lead spheres
2	2584	2x heat capacity	0.854	0.0166	34.0	greatly increased COP
3	2585	<i>Same as 2583, except Th=30 K</i>	<i>0.498</i>	<i>0.0311</i>	<i>42.4</i>	<i>increased Qnet</i>
4	2586	<i>Same as 2585, decrease length</i>	<i>0.431</i>	<i>0.0277</i>	<i>17.7</i>	<i>slight decrease COP</i>
5	2587	<i>Same as 2585, decrease At</i>	<i>0.445</i>	<i>0.0271</i>	<i>16.7</i>	<i>almost no change</i>
6	2588	<i>Same as 2587, increase Dh</i>	<i>0.471</i>	<i>0.0290</i>	<i>17.2</i>	<i>slight improvement</i>
7	2589	Same as 2583, except Er3Co	0.953	0.0221	37.1	big improvement
8	2590	Increase cond. fact. to 0.2	0.841	0.0195	36.9	small degradation
9	2591	Constant Cm=0.6	-0.208		33.7	poor performance ??
10	2592	<i>Same as 2585, except Er3Co, Th=30 K</i>	<i>1.548</i>	<i>0.0895</i>	<i>46.8</i>	<i>big improvement</i>
11	2593	<i>Decrease L</i>	<i>1.436</i>	<i>0.0885</i>	<i>21.9</i>	<i>big decrease in f</i>
12	2606	<i>Same as 2593 except P0=2 MPa</i>	<i>1.636</i>	<i>0.103</i>	<i>19.8</i>	<i>big improvement</i>
13	2607	<i>Increase f to 45 Hz</i>	<i>1.454</i>	<i>0.0888</i>	<i>33.2</i>	<i>some degradation</i>
14	2608	<i>Like 2593 except decrease At and L</i>	<i>1.488</i>	<i>0.0888</i>	<i>20.5</i>	<i>about same as 2593</i>
15	2609	<i>Er(0.2)Dy(0.8)Ni(2)</i>	<i>1.171</i>	<i>0.0717</i>	<i>19.1</i>	<i>some degradation</i>
16	2610	<i>Cm=0.2+0.025T</i>	<i>1.682</i>	<i>0.0902</i>	<i>23.6</i>	<i>better than 2608</i>
17	2611	Tc=30 K, Th=80 K, lead spheres ok			9.197 0.126 19.2	
18	2612	Like 2590 except decrease At	0.985	0.0222	22.6	better than 2590
19	2613	Like 2590 no change	0.818	0.0190	36.8	same as 2590
20	2614	Like 2590 except P0=2 MPa	0.533	0.0115	27.4	worse than 2590
21	2615	Like 2611 except increase At and L			11.90 0.158	
37.7		slightly better system				
22	2616	Like 2590 except P0=2.5 MPa	0.672	0.0151	33.0	worse than 2590
23	2617	Like 2590 except Pratio=1.25	0.530	0.0147	31.4	worse than 2590
24	2618	Like 2612 except decrease At	0.923	0.0197	13.7	slightly worse than 2612
25	2619	Like 2612 except 1.5xCm	0.852	0.0167	20.2	worse than 2612, ??
26	2620	Like 2618 except increase Dh to 40.9 μ m	-0.282		12.4	poor performance
27	2624	Like 2612 except 0.75xCm	0.822	0.0211	24.8	slightly worse than 2612
28	2625	Like 2620 except f=45 Hz	-0.261		24.8	poor, need smaller Dh
29	2626	Like 2620 except decrease ng, increase At	-0.48		10.7	poor, need smaller Dh
30	2627	Like 2620 except increase Dh	-1.8		11.9	poor need smaller Dh
31	2628	Like 2620 except screens Dh=39, lower At	0.250	0.0087	16.4	better than 2620 ??
32	2629	Like 2612 except 1.3xCm	0.940	0.0232	21.1	about same as 2612
33	2630	Like 2612 except lower At	0.988	0.0216	17.9	about same as 2612
34	2631	Like 2612 except f=45 Hz	0.705	0.0148	36.1	worse than 2612
35	2632	Like 2612 except f=60 Hz	0.370	0.0071	45.3	much worse than 2612
36	2633	Like 2612 except ng=0.30, higher At	0.959	0.0189	20.7	worse than 2612
37	2634	Like 2612 except lead	0.287	0.0071	22.5	much worse than 2612
38	2635	Like 2631 except smaller L, 45 Hz	0.510	0.0116	30.8	worse than 2631
39	2636	Like 2612 except phase=0	0.674	0.0138	33.0	worse than 2612
40	2637	Like 2612 except increase ng, decrease At	0.763	0.0197	24.8	worse than 2612
41	2638	Like 2612 except screen, increase L	0.320	0.0112	27.8	much worse than 2612
42	2639	Finer screen, increase At, decrease L	0.316	0.0112	27.2	same as 2638
43	2640	Like 2634 except 1.5xCm	0.742	0.0153	21.0	much better than 2634
44	2641	Like 2612 except parallel plates	0.468	0.0123	23.1	worse than 2612

45	2642	Like 2641 except cond. factor = 0.2	0.976	0.0251	24.4	better than 2612, spheres
45a	2642a	Like 2642 except 40 points	0.965	0.0252	23.5	same as 2642
46	2643	Like 2642 except Dh=25 (reduced)	1.382	0.0362	24.6	better than 2642 & 2612
46a	2643a	Like 2643 except 40 points	1.317	0.0340	24.0	slightly lower than 2643
47	2644	Like 2634 except 2xCm	0.997	0.0188	20.1	slightly worse than 2612
48	2645	Like 2638 except lead screen	-0.386	-0.0143	25.3	poor
49	2648	Like 2643 except Dh=20 (reduced)	1.383	0.0361	25.1	same as 2643
49a	2648a	Like 2648 except 40 points	1.309	0.0336	24.2	=2643a, lower than 2648
50	2649	Like 2643a except neodymium	0.702	0.0193	23.6	worse than 2643a
51	2650	Like 2612 except phase = 0	0.912	0.0187	34.1	worse than 2612 (>2636)

Table 3. General Trends (10 K to 80 K)

Spheres

1. Effect of matrix heat capacity:

- Runs 2583, 2584, 2589, 2590, 2591, 2619, 2624, 2629, 2634, 2640
 - Er₃Co much better than lead sphere (2612 & 2634)
 - 0.75x, 1x, 1.3x, 1.5x, Cm of Er₃Co shows little improvement beyond 1x (2612, 2619, 2624, 2629)

2. Effect of hydraulic diameter Dh:

- Runs 2618, 2620
- Dh = 32.7 μm (80 μm spheres) much better than Dh = 40.9 μm (100 μm spheres)

3. Effect of length L:

- Not studied

4. Effect of cross-sectional area At:

- Runs 2590 (At/*m* = 0.77 cm²·s/g), 2612 (0.51 cm²·s/g), 2630 (0.43 cm²·s/g)
- 0.77 to 0.51 gives big improvement; almost no change to 0.43 (but φ lower)

5. Effect of average pressure P0:

- Runs 2590 (P0 = 3.0 MPa), 2614 (2 MPa), 2616 (2.5 MPa):
- COP steadily increases from 0.0115 to 0.0195 as P0 increases from 2.0 to 3.0 MPa
- φ increases from 27.4 to 36.9 as P0 increases from 2.0 to 3.0 MPa
- 3.0 MPa appears to be best P0

6. Effect of pressure ratio Pr:

- Runs 2590 (Pr = 1.30), 2617 (1.25)

- COP increases from 0.0147 to 0.0195 as Pr increases from 1.25 to 1.30
- ϕ increases from 31.4 to 36.9 as Pr increases from 1.25 to 1.30
- Pr = 1.30 appears to be better overall than 1.25

7. Effect of frequency f:

- Runs 2612 (f = 30 Hz), 2631 (45 Hz), 2632 (60 Hz)
- COP decreases steadily from 0.0222 to 0.0071 as f increases from 30 to 60 Hz

8. Effect of porosity ng:

- Runs 2612 (ng = 0.38), 2633 (0.30), 2637 (0.45)
- COP is maximum at ng = 0.38, small decrease on each side

9. Effect of phase between \dot{m}_c and P:

- Runs 2612 (-15°), 2636 (0°), 2650 (0°)
- COP decreases from 0.0222 to 0.0138 as phase changes from -15° to 0°

Parallel plates

1. Effect of material (Cm):

- Runs 2643a (Er3Co) and 2649 (Nd)
- COP decreases from 0.0340 to 0.0193 when going from Er3Co to Nd

1. Effect of Dh (tg = Dh/2):

- Runs 2642a (Dh = 32.7 μm), 2643a (25 μm), 2648a (20 μm)
- COP increases from 0.0252 to 0.0340 as Dh decreases from 32.7 μm to 25 μm
- COP and Qnet do not change as Dh decreases from 25 μm to 20 μm
- Tmid decreases significantly as Dh decreases from 32.7 to 20 μm (significance ??)

2. Effect of conduction factor kf

- Runs 2641 (kf = 1.0), 2642 (0.2)
- COP increases from 0.0123 to 0.0251 as kf decreases from 1.0 to 0.2

Screens

1. Effect of material (Cm):

- Runs 2638 (Er₃Co) and 2645 (lead)
 - COP decreases from 0.0112 to -0.0143 in going from Er₃Co to lead

2. Effect of mesh (Dh):

- Runs 2638 (500 mesh, Dh = 39.3 μm), 2639 (30 μm)
- No change in COP (0.0112)

Comparison of Geometries

- Runs 2612 (spheres), 2638 (screen), 2641 (parallel plates, kf=1.0), 2642 (parallel plates, kf=0.2)
- Screen COP = 0.0112; sphere COP = 0.0222; plate COP = 0.0251 (kf=0.2); plate COP = 0.0123 (kf=1.0)
- For optimum Dh in plates use run 2643a (Dh = 25 μm); plate COP = 0.0340 (kf=0.2)

Summary of best performance

1. Parallel plates (**best overall performance**) run 2643a, COP = 0.0340, $\phi = 24.0^\circ$

P0 = 3.0 MPa

Pr = 1.3

f = 30 Hz

Er₃Co

Dh = 25 μm (tg = 12.5 μm, **very difficult**)

ng = 0.38 (**have not studied effect of ng in plates yet**)

L = 35 mm

$At/\dot{m}_c = 0.51 \text{ cm}^2 \cdot \text{s/g}$

kf = 0.2 (must provide some gaps)

2. Packed spheres (**best practical geometry**) run 2612, COP = 0.0222, $\phi = 22.6^\circ$

P0 = 3.0 MPa

Pr = 1.3

f = 30 Hz

Er₃Co

Dh = 32.7 μm (80 μm spheres)

ng = 0.38

L = 35 mm

$At/\dot{m}_c = 0.51 \text{ cm}^2 \cdot \text{s/g}$

Kf = 0.2

The use of 80- μm diameter spheres can present some problems in confining such small particles within the regenerator. If they escape and travel to the compressor, they can damage the compressor. We are considering sintering the spheres or bonding them together with a thin epoxy layer a few micrometers thick.

In the modeling done here the losses within the regenerator are modeled fairly accurately. Many years of experience and comparisons with experiments, including some at 10 K with 2.5 Hz frequency, indicate that REGEN3.1 calculates these losses quite accurately. However, the losses within the pulse tube are not well understood and currently cannot be modeled accurately. The refrigeration reduction factor used with REGEN3.1 represents an empirical factor that we use to account for losses within the pulse tube. For a pulse tube refrigerator this factor is the figure of merit *FOM* of the pulse tube, defined as

$$FOM = \frac{\langle \dot{H} \rangle}{\langle P\dot{V} \rangle}. \quad (3)$$

Measured values for *FOM* range from about 0.55 to 0.85 in small pulse tubes [4] to as high as 0.96 in very large pulse tubes where acoustic streaming was eliminated with a slight taper [5]. These values of *FOM* are then used as empirical factors in calculations of pulse tube performance. At a temperature of 10 K real gas effects become very important and the *FOM* in Eq. (3) should be modified to

$$FOM = \frac{\langle \dot{H} \rangle - \langle \dot{H}_P \rangle}{\langle P\dot{V} \rangle - \langle \dot{H}_P \rangle}, \quad (4)$$

where $\langle \dot{H}_P \rangle$ is the time-averaged isothermal enthalpy flow due to pressure changes in a real gas. For an ideal gas this term is zero because the enthalpy of an ideal gas is independent of pressure.

For the second stage we used a *FOM* of 0.8 in all of the REGEN3.1 calculations performed here. Run #2612 was found to give the optimum performance for a packed sphere bed in the second stage. As will be discussed later a *FOM* of about 0.8 is needed for the second stage in order for the system to have good efficiency. For the first stage a more conservative *FOM* of 0.7 was used. Run #2655 gave the optimum performance in the first stage for the conditions imposed on it by the second stage. Stainless steel screen was used for all first stage runs. Screen has been found from many previous runs to give excellent performance for these higher temperatures. Spheres are needed for the second stage because the optimum porosity decreases as the temperature is lowered. For screen the porosity is about 0.686 whereas for spheres the porosity is 0.38. Conductivity degradation factors for stacked screen and packed spheres are based upon measurements carried out at NIST for these factors. Figure 8 compares the entropy produced by the net refrigeration and all the losses in the cold head for the first and second stages. The entropy is normalized by the total entropy flow available at the warm end of each regenerator. Note that the net refrigeration power of the second stage represents a rather small fraction (14%) of the total power available. As a result, a small change in either the regenerator or pulse tube losses would have a large effect on the net refrigeration. Figure 8 shows that the net refrigeration of the first stage is a greater fraction (37%) of the total power available to that stage.

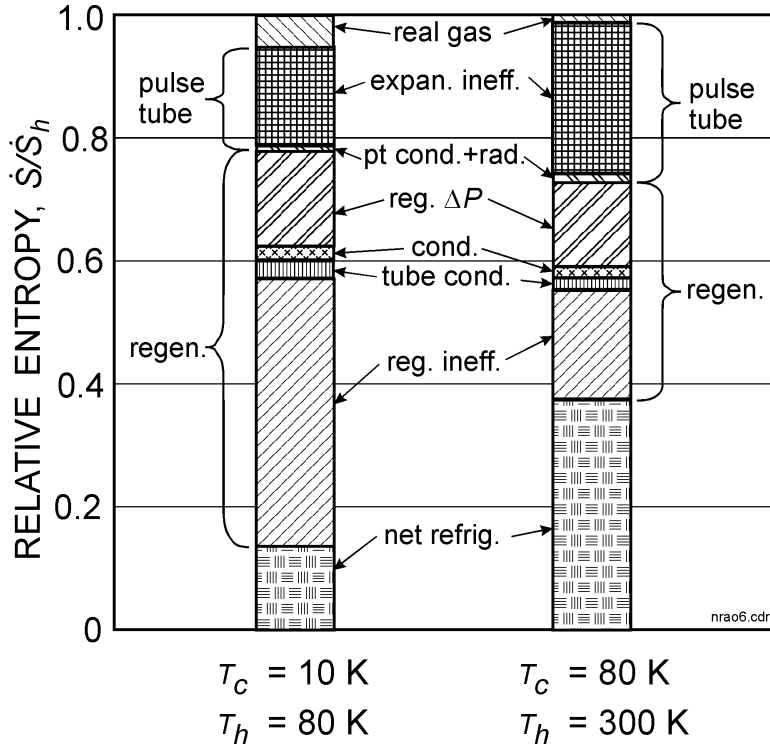


Figure 8. Relative entropy production from losses and net refrigeration in each stage of pulse tube cryocooler.

The *FOM* of the second stage would most likely be influenced by the temperature of the warm end of the second-stage pulse tube. A lower temperature should lead to a higher *FOM*. Thus, we investigated the effect of having the warm end heat sink to the first stage and varying the temperature of the first stage between 65 and 80 K. For the particular set of specifications for this refrigerator, it appears that having the warm end at about 80 K is about the optimum. Certainly during the experimental phase of the program we plan to measure the performance as a function of the second-stage warm end temperature.

Effect of *FOM* on overall performance. The *FOM* of the second stage is probably the one loss with the largest uncertainty and it has a significant effect on the net refrigeration power. A computer program was written to study the effect of the *FOM* of the second stage on the overall input PV power for the two-stage refrigerator to produce the required net refrigeration power at both stages. It uses as input the specific performance factors determined from the REGEN3.1 calculations. The program was also used to study the effect of the warm end temperature of the second stage pulse tube. A REGEN3.1 calculation can be applied to any size refrigerator as long as the ratio of flow to cross-sectional area is kept constant. We then normalize the REGEN3.1 output to allow it to be applied to any system size. For example, the denominator of Equation (4), to be known as the modified PV power at the cold end of the regenerator, is used for normalizing the losses of each stage. The *FOM* is already defined as the normalized pulse tube loss. We let q be the normalized losses of a regenerator. These losses include those from regenerator ineffectiveness, conduction through the matrix and the tube, and radiation, but not that associated with the pressure drop. The effect of the pressure drop is accounted for by using

the ratio w , defined as the ratio of modified PV power at the warm end of the regenerator to the modified PV power at the cold end.

We begin the derivation by noting that the net refrigeration power of the second stage can be expressed as

$$\dot{Q}_{net2} = (FOM_2 - q_2)\dot{W}_{c2m}, \quad (5)$$

where \dot{W}_{c2m} is the modified PV power at the cold end of the second stage. In the first stage the modified PV power at the cold end is divided between the first-stage pulse tube and the second-stage regenerator. The refrigeration power produced by the first-stage pulse tube is given by

$$\dot{Q}_{ref} = FOM_1(\dot{W}_{c1m} - w_2\dot{W}_{c2m}), \quad (6)$$

where the term in parentheses represents the modified PV power flowing in the first stage pulse tube. The net refrigeration power of the first stage then becomes

$$\dot{Q}_{net1} = \dot{Q}_{ref} - (q_1 + q_{pt})\dot{W}_{c1m} = FOM_1(\dot{W}_{c1m} - w_2\dot{W}_{c2m}) - (q_1 + q_{pt})\dot{W}_{c1m}, \quad (7)$$

where q_{pt} is the heat rejected to the first stage by the warm end of the second-stage pulse tube and normalized by the PV power flow at the cold end of the first-stage regenerator. This term is zero if the warm end of the second stage pulse tube is heat sunk to ambient. The heat rejected at the warm end of the second-stage pulse tube is given by

$$\dot{Q}_{pt} = (FOM_2)\dot{W}_{c2m} = q_{pt}\dot{W}_{c1m}. \quad (8)$$

Thus, q_{pt} can be expressed as

$$q_{pt} = (FOM_2)\dot{W}_{c2m} / \dot{W}_{c1m}. \quad (9)$$

Equations (5) and (7) can be rearranged to give

$$\dot{W}_{c2m} = \dot{Q}_{net2} / (FOM_2 - q_2) \quad (10)$$

and

$$\dot{W}_{c1m} = \frac{\dot{Q}_{net1} + FOM_1 w_2 \dot{W}_{c2m}}{FOM_1 - q_1 - q_{pt}}. \quad (11)$$

The term q_{pt} can be derived by iteration from the known quantities using Equations (9), (10), and (11). According to the definition of w the modified PV power at the warm end of the first-stage regenerator is given by

$$\dot{W}_{h1m} = w_1 \dot{W}_{c1m}. \quad (12)$$

The PV power flow at the warm end of the first stage is given as

$$\dot{W}_{h1} = \dot{W}_{h1m} + \langle \dot{H}_{p1} \rangle = (1 + h_{p1})\dot{W}_{h1m}, \quad (13)$$

where h_{p1} is the ratio of isothermal enthalpy flow due to pressure variations to the modified PV power at the warm end. Substituting Equations (10), (11), and (12) into Equation (13) yields

$$\dot{W}_{h1} = \frac{(1 + h_{p1})w_1 \{ \dot{Q}_{net1} + FOM_1 w_2 [\dot{Q}_{net2} / (FOM_2 - q_2)] \}}{FOM_1 - q_1 - q_{pt}}, \quad (14)$$

where q_{pt} is evaluated from Equation (9). From Equation (14) we see that the input PV power required to provide for the second stage cooling is given by

$$\dot{W}_{h1Q2} = \frac{(1 + h_p)w_1 FOM_1 w_2 [\dot{Q}_{net2} / (FOM_2 - q_2)]}{FOM_1 - q_1}. \quad (15)$$

The term q_{pt} was excluded from the denominator of Equation (15) to give the input power needed only by the second stage whether it is rejecting heat to ambient or to the 80 K first stage.

In these last two equations the input values are the two net refrigeration terms ($\dot{Q}_{net2} = 2 \text{ W}$, $\dot{Q}_{net1} = 16 \text{ W}$) that have been previously specified. All other quantities are dimensionless terms that are determined from the optimized REGEN3.1 runs for each stage. Because they are dimensionless terms, the REGEN3.1 runs need not be for the specific size system needed here. Values of these dimensionless terms are: $FOM_2 = 0.8$, $q_2 = 0.624$, $w_2 = 8.28$, $FOM_1 = 0.7$, $q_1 = 0.263$, $w_1 = 4.215$, and $h_{p1} = 0.014$.

Figure 9 shows how the system input power varies with the FOM of the second stage when the warm end of the second-stage pulse tube is heat sunk to ambient and when it is heat sunk to the 80 K first stage. The solid line in this graph indicates the input power needed to drive only the second stage, as given by Equation (15). It includes the power needed by the first stage to intercept the regenerator loss caused by mass flow in the first stage required to drive the second stage. It does not include the input power needed by the first stage to accept the heat rejected at the warm end of the second-stage pulse tube when it is heat sunk to the first stage. Note from Figure 9 that the second stage requires most of the input power. It is a result of the high relative losses given by q_2 being quite close to the relative available refrigeration given by FOM_2 . Heat sinking the second-stage pulse tube to the first stage causes the input PV power to change from 800 W to 900 W for $FOM_2 = 0.8$. However, if the reduced warm end-temperature of the second-stage pulse tube increases FOM_2 from 0.8 to 0.85, the input power becomes about 650 W. Only experiments can resolve this question about the actual values of the FOM since there are no models that can accurately predict these values.

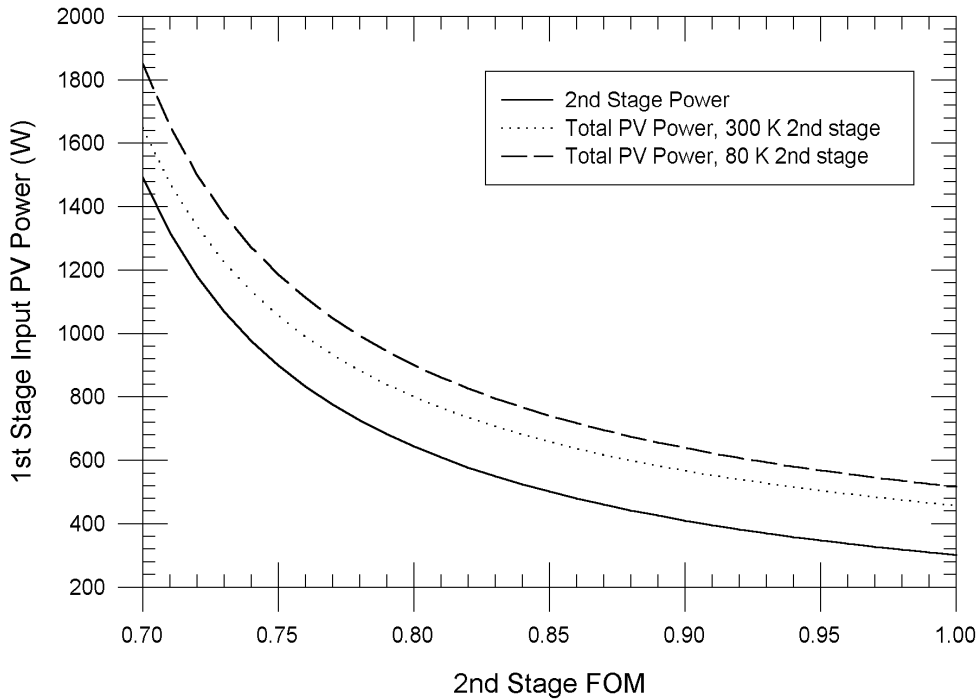


Figure 9. Input PV power as a function of the 2nd stage figure of merit.

Optimized System Design and Performance. Table 4 lists the geometry of the regenerators, pulse tubes, heat exchangers, inertance tubes, and reservoir volumes for the optimized system. The inertance tube for each stage is given as a double diameter tube. The use of two diameters as opposed to one diameter increases the phase shift by about 10 degrees. The phase shift of 46° for the second stage is very close to the desired value of 54°. We expect in practice to achieve the larger phase shift, since we have found that our model under-predicts the phase shift by a few degrees. Thus, a secondary orifice is not required for the second stage. That eliminates the possibility of DC flow in that stage. The first-stage inertance tube provides a phase shift of 31°, which is significantly less than the desired value of 49°. Thus, a secondary orifice is required for the first stage to provide the additional phase shift. The design values of 2 W at 10 K and 16 W at 80 K are actually input values for the optimized design.

The input PV power is calculated to be 900 W with the warm end of the second-stage pulse tube heat sunk to 80 K, which is estimated to be the optimum configuration. This value of 900 W does not take into account any losses in the room-temperature components, such as the transfer

Table 4. Geometry of Refrigerator Components

Component	OD (mm)	ID (mm)	Length (mm)	Matrix
Second Stage:				
Regenerator	28.6	27.8	35.0	Er ₃ Co and Pb+5%Sb (80 μm)
Pulse tube	11.1	10.7	54.4	
Cold heat exchanger	11.1		7.37	150 mesh copper screen
Warm heat exchanger	11.1		6.66	150 mesh copper screen
Inertance tube I		2.20	1.27 m	(θ = 46°)
Inertance tube II		2.60	1.81 m	
Reservoir volume				200 cm ³
First Stage:				
Regenerator	50.6	49.4	45.0	400 mesh stainless screen
Pulse tube	15.9	15.1	128	
Cold heat exchanger	15.9		12.66	150 mesh copper screen
Warm heat exchanger	15.9		11.63	150 mesh copper screen
Inertance tube I		3.00	2.02 m	(θ = 31.3°)
Inertance tube II		3.90	3.69 m	
Reservoir volume				1000 cm ³
First Stage for Second-Stage Test				
Regenerator	34.9	33.9	45.0	400 mesh stainless steel

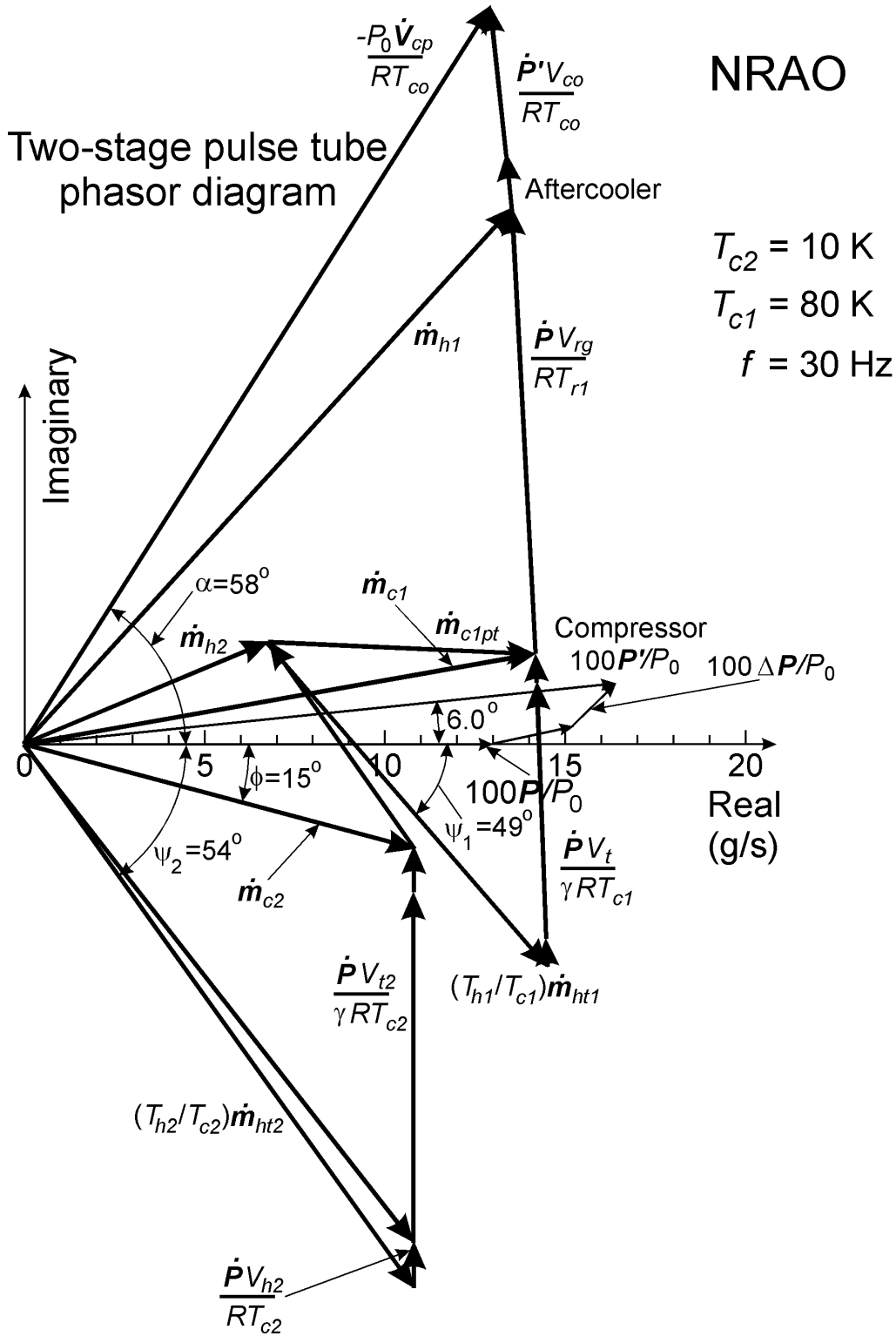
line and irreversible effects within the compressor. Those losses could amount to at least 200 W. The total input PV power would be at least 1100 W. Another 100 W may be consumed by the flow to the secondary orifice of the first stage. With an 85% efficient compressor the input electrical power becomes 1400 W. Thus, these calculations are very encouraging in the sense that the input power should be less than the maximum acceptable value of 2000 W.

Figure 10 shows the phasor diagram for all the mass flows and the rate of change of mass within the various components. On the same diagram the pressure phasors are shown multiplied by a scale factor to be able to use the same numbers on the axes. This phasor diagram indicates what phase angles are needed between mass flow and pressure at the warm end of the two pulse tubes. Such phase angles are achieved by the use of inertance tubes. The geometry of the inertance tubes were calculated by our model based on a transmission line analogy. The phasor diagram also indicates that the phase between the negative of the volume flow rate and the pressure in the compressor is $58.0 - 6.0 = 52$ degrees. This phase angle is an input to the compressor manufacture in the design of the compressor in order to match the power and acoustical impedance of our pulse tube system. The acoustical impedance is given by the complex ratio of the pressure to the volume flow rate. For a compressor temperature of $T_{co} = 320$ K the swept volume from the phasor diagram is 61 cm^3 . When pseudo-adiabatic compression is used instead of isothermal compression in the phasor diagram and flow to the secondary orifice is taken into account, the compressor swept volume increases to about 80 cm^3 .

Figure 11 shows the layout drawing of the two-stage system. The system is designed with flanged joints and indium wire seals to allow for using various regenerators or pulse tubes. The heat sinking of the second-stage pulse tube to the first stage is carried out with some allowance for differential thermal contraction between the various components. During initial testing of the second stage regenerator and pulse tube, the first-stage pulse tube will be replaced with a thermal link to a Gifford-McMahon refrigerator. In that situation the first-stage regenerator will be one with a smaller diameter in order to scale with the reduced mass flow in the absence of the first-stage pulse tube.

Linear Flexure Bearing Compressor. NIST has on order a linear compressor from CFIC designed specifically for this application. It is a dual opposed-piston design based on their common 2 kW Star motor design. The dual opposed-piston design will produce negligible compressor vibration. This design is shown in Fig. 12. More than 30 of the 2 kW single-piston compressors are currently in operation, giving us great confidence in the operating lifetime. The Star motor design uses simple block magnets in a unique design that provides low cost and easy assembly. The moving mass is supported on flexure bearings that cause no axial rotation while providing the required radial and torsional stiffness. The flexure bearings support a clearance seal between the piston and cylinder, which leads to a design with no rubbing parts. Thus, lifetimes should be very long, and no oil lubrication is required.

NRAO

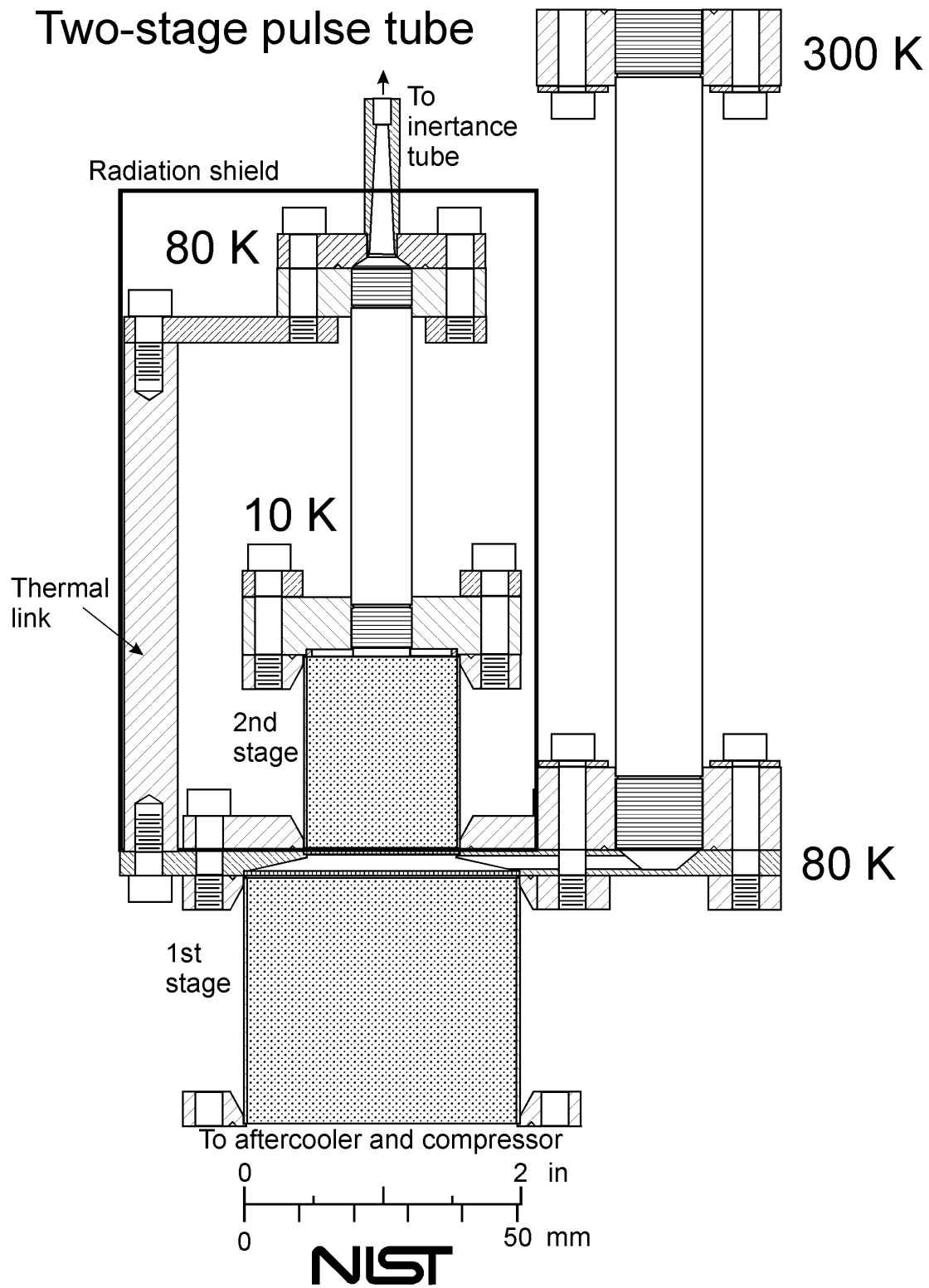


10/17/99
 NRAO/phasor1.cdr
 NIST

Figure 10. Phasor diagram of optimized two-stage pulse tube for 10 K operation.

NRAO

Two-stage pulse tube



Pulse tube layout1.cdr

Figure 11. Layout drawing of NRAO two-stage pulse tube refrigerator.

Some key design features of the Star motor are:

- Minimal magnetic side pull - Short, solidly supported magnets allow close operating clearances. Radial plunger stability is enhanced by equal magnet and iron face areas.
- Stacked laminations perpendicular to the axis allow low-cost production
- Multiple bobbin-wound coils - One coil slides on to each of the eight salient poles. This modular coil concept allows normal automatic winding equipment to be used.
- Exposed coils provide excellent cooling - This allows higher magnet loading for normal ambient temperature operating environments.
- Cost-effective rectangular block magnets - Each magnet is bonded onto a rigid hub (8 magnets per hub) and mechanically secured.
- Unique single air gap design – The motor design has only a single air gap in its magnetic circuit, reducing leakage flux.
- Infinite life flexure bearings - The low magnetic side pull forces uniquely intrinsic to the STAR enable use of light-gage flexure bearings.

The nominal compressor design for this application provides 1400 W of PV power at 30 Hz. It has a 100 cm³ swept volume, and it is designed to resonate at 30 Hz with a 1.45 pressure ratio and 2.5 MPa average pressure. It can operate at higher pressures, with a minimum requirement of 3.0 MPa pressure. At a pressure of 3 MPa the swept volume needs to be reduced to 84 cm³, which is still greater than the required amount of 80 cm³. It will have position sensors allowing us to measure PV power to fully characterize pulse tube systems. The compressor will have an adjustable moving mass, allowing us to operate at higher frequencies if desired. At 60 Hz operation the PV power should be 2800 W.

Vacuum System. The vacuum system consists of a chamber that is supported by a rack system and bench with a lift hoist and chamber rotation mechanism. The primary goal is to place the compressor and pulse tube refrigerator entirely within the vacuum chamber for these laboratory tests. For a field installation the compressor would be mounted outside any vacuum chamber.

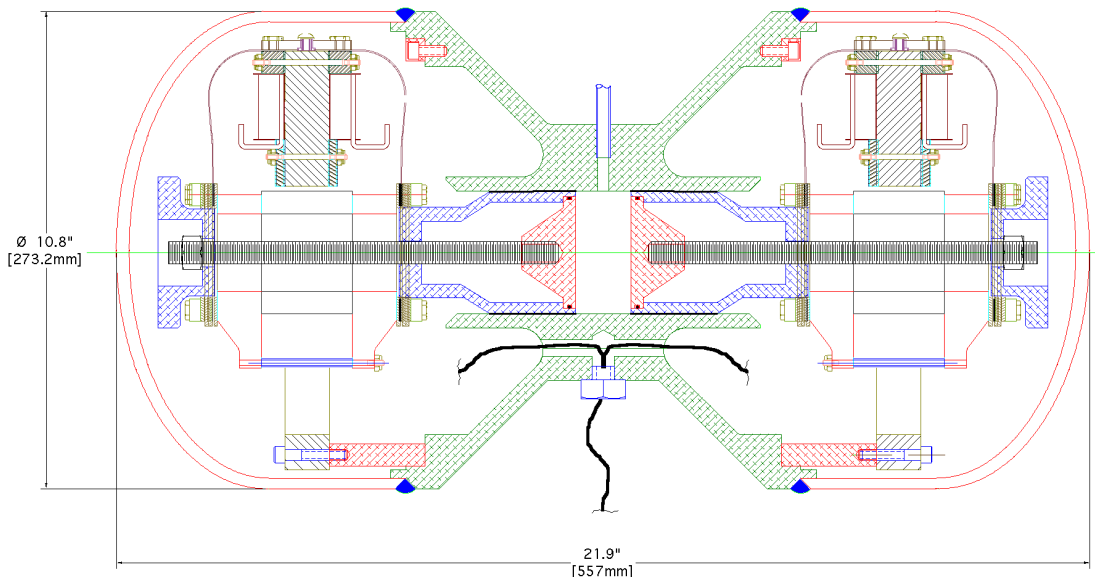


Figure 12. Cutaway view of CFIC flexure-bearing compressor.

To mount the compressor inside the vacuum chamber leads to the size requirements for the chamber. The specified size is 660 mm (26") in diameter and 610 mm (24") in length connected to a feedthrough collar of the same diameter that is 152 mm (6") tall with plates at each end, thus creating a 762 mm (30") tall chamber. This system concept is shown in Figure 13. There are four viewing ports, which allow for both visual as well as physical access to the chamber.

The feedthrough collar provides two important functions. First, the collar provides the capability to feed through connections into the chamber. Second, the collar provides the structural backbone and axis for rotation of the chamber. Ten KF50 ports route all electrical power, cooling, sensors, and rough pump connections out of the chamber without going through either endplate. This allows all of the connections to remain in place while working on the pulse tube system with the 610 mm (24") tall chamber and endplate removed for access. Additionally, the main plate and collar can be rotated by the rotation mechanism if necessary with all feed through connections in place.

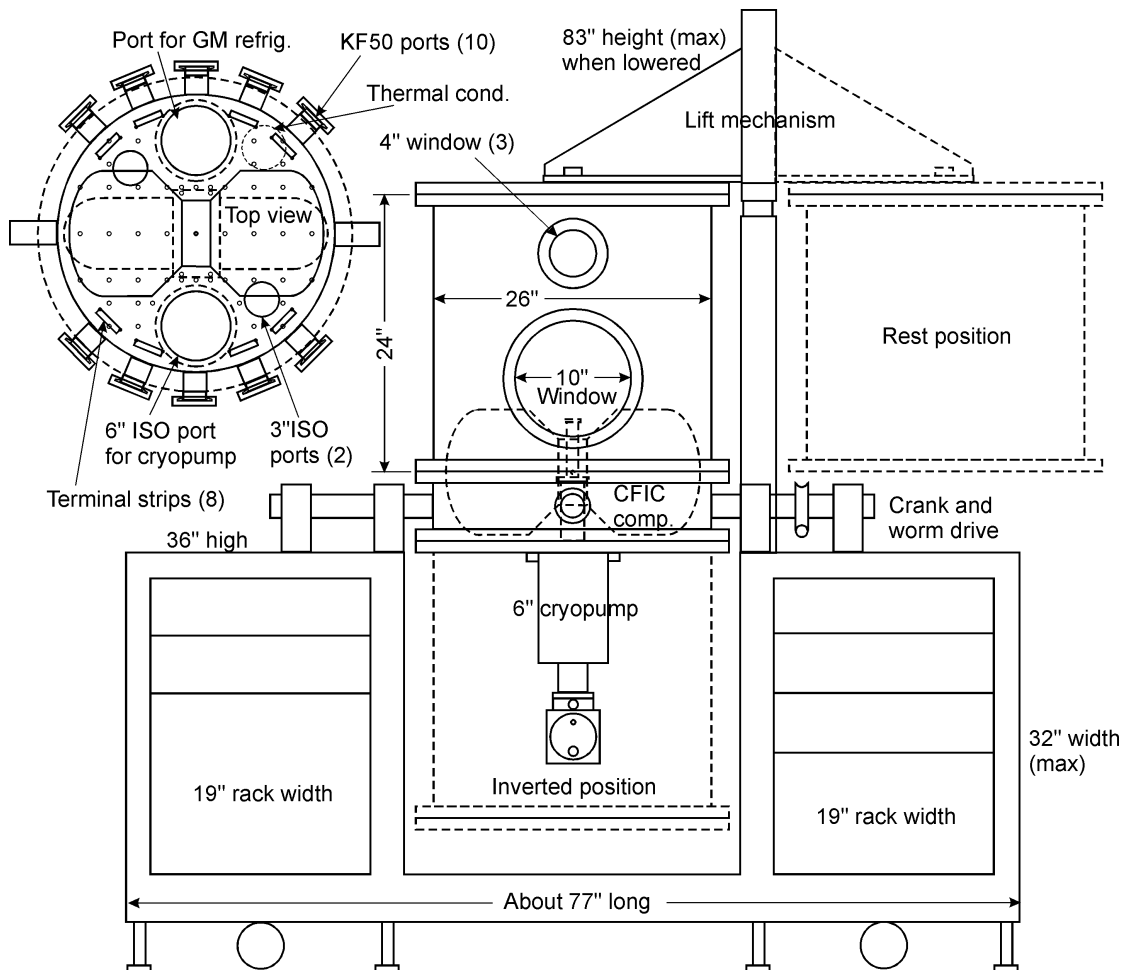


Figure 13. Vacuum chamber, support bench, and lift mechanism for pulse tube testing.

The main end plate attached to the feedthrough collar supports the pulse tube system as well as the system cryopump and Gifford-McMahon refrigerator while carrying out subsystem tests. A bolt-hole grid work offers a wide variety of attach points within the vacuum space for other necessary equipment. There are also two 75 mm (3") ISO ports that can be used to attach or feedthrough other hardware needed if the 10 KF50 feedthrough collar ports prove insufficient. In the event the compressor needs to be operated external to the vacuum space, the ambient side of the end plate has attach points as well. All of these details are represented in Figures 13 and 14.

The rack system and bench with lift hoist and chamber rotation mechanism are shown in the system concept of Figure 13. It is comprised of three main elements: (a) the rack with two standard width bays for electronics, (b) the hoist mechanism to lift and rotate the chamber off of the feedthrough collar, and (c) the chamber rotation mechanism to rotate the entire chamber and attached hardware about the collar axis at 5 degree increments with a maximum rotation of at least 180 degrees from the vertical. The vacuum chamber and support bench have been ordered and delivery is expected by the end of 1999.

Conclusions. The calculations based upon our most accurate and current models predict that the cooling requirements specified for the two-stage pulse tube refrigerator can be met with a 30 Hz pulse tube system. The calculated input electrical power is about 1300 to 1400 W, assuming the compressor operates at an efficiency of 85%, which is normal efficiency for the compressor we

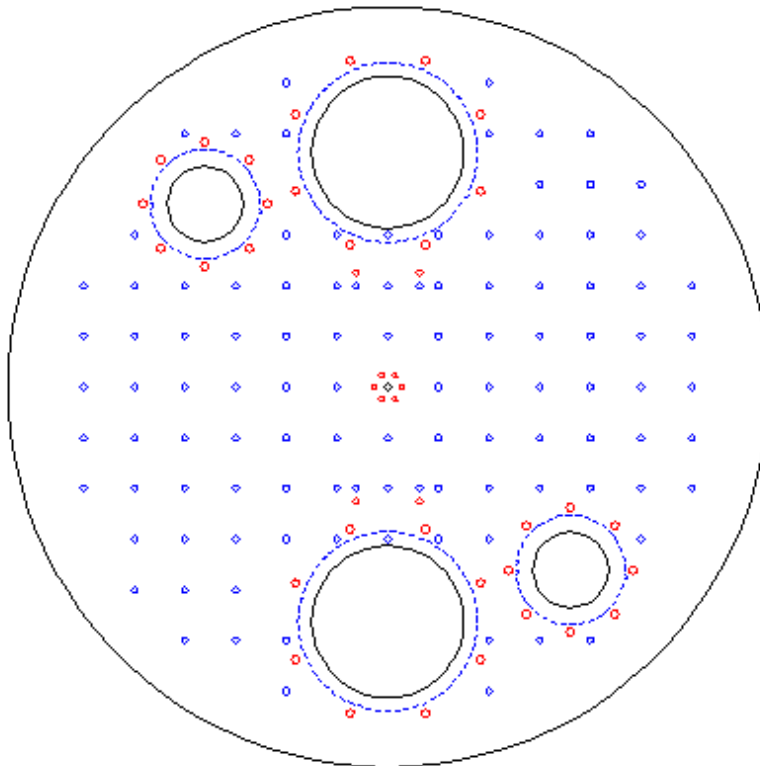


Figure 14. Layout of base plate in vacuum chamber.

have ordered. The calculations depend very much on the figure of merit in the second-stage pulse tube. We have used a *FOM* of 0.80 in the calculations. Higher values have been achieved at higher temperatures in one-stage systems. For example, we recently achieved a *FOM* of 0.88 in an oxygen liquefier that produced 20 W at 90 K. No experiments have been done at temperatures near 10 K. Thus, the experiments planned for the next phase of this research will include measurements of the *FOM* of the second-stage pulse tube and the effect that various parameters have on this value.

References.

1. R. Radebaugh, Advances in Cryocoolers, Proc. ICEC16/ICMC, Japan, 1996, Elsevier Science, Oxford (1997) pp. 33-44.
2. R. Radebaugh, A review of pulse tube refrigeration, Adv. in Cryogenic Engineering, Vol.35, Plenum Press, New York (1990) pp. 1191-1205.
3. R. Radebaugh, Development of the pulse tube refrigerator as an efficient and reliable cryocooler, Proc. Institute of Refrigeration (London), Vol. 1999-00, to be published.
4. W. Rawlins, R. Radebaugh, P. E. Bradley, and K. D. Timmerhaus, Energy flows in an orifice pulse tube refrigerator, Adv. in Cryogenic Engineering, Vol. 39, Plenum Press, New York (1994) pp. 1449-1456.
5. G. W. Swift, M. S. Allen, and J. J. Wollan, Performance of a tapered pulse tube, *Cryocoolers 10*, Kluwer Academic/Plenum Press, NY (1999) pp. 315-320.